Hindawi
Journal of Nanomaterials
Volume 2017, Article ID 6286549, 10 pages
https://doi.org/10.1155/2017/6286549

Research Article

One-Step Synthesis of Hierarchical Micro-Mesoporous SiO_2/Reduced Graphene Oxide Nanocomposites for Adsorption of Aqueous Cr(VI)

Guiyun Yi, Baolin Xing, Huihui Zeng, Xiaodong Wang, Chuanxiang Zhang, Jianliang Cao, and Lunjian Chen

College of Chemistry and Chemical Engineering, Henan Polytechnic University, Jiaozuo 454003, China

Correspondence should be addressed to Baolin Xing; baolinxing@hpu.edu.cn

Received 5 February 2017; Revised 3 May 2017; Accepted 22 May 2017; Published 24 July 2017

Academic Editor: Ilker S. Bayer

A novel micro-mesostructured SiO_2/reduced graphene oxide (RGO) nanocomposite was successfully synthesized by means of simple one-step hydrothermal method under acidic conditions using tetraethoxysilane (TEOS) and graphene oxide (GO) as the raw material. The nanocomposites were characterized by TEM, XRD, FT-IR, TG-DSC, and N_2 adsorption-desorption. The results showed that GO was partially reduced to RGO without adding any reducing agent and SiO_2 nanoparticles (ca. 10 nm) were uniformly anchored on the surface of RGO. The optimized composite contained 75 wt.% SiO_2 and possessed hierarchical micro-mesoporous structure with surface area of 676 m^2/g. The adsorption performance of synthesized SiO_2/RGO samples was investigated by removal efficiency of Cr(VI) ions in wastewater. The Cr(VI) adsorption reached equilibrium in 30 min and 98.8% Cr(VI) adsorption efficiency was achieved at pH = 2 at 35°C. Stability tests showed that SiO_2 nanoparticles effectively prevented RGO from the restacking. The mechanisms of composite formation and for Cr(VI) adsorption were suggested.

1. Introduction

Graphene has attracted significant research attention since its first report in 2004 [1], owing to the unique two-dimensionally hexagonal structure [1] and extraordinary properties [2–4]. Graphene has been known as promising adsorbent with great potential in wastewater treatment [5–7] because of its large theoretical surface area (2630 m^2/g) [8], remarkable electronic properties [9] and mechanical properties [10], and high ability of modification [11, 12]. However, it is difficult to disperse graphene in water due to its hydrophobicity, agglomeration, and restacking [13–15], limiting its use in aqueous systems for decontamination.

Graphene oxide (GO), a highly oxidative form of graphene containing of a variety of oxygen functional groups, can solve the problem because it has similar properties to graphene but is more hydrophilic, which is a prerequisite as adsorbent used in aqueous system [16–18]. However, GO has very weak binding affinity for anionic compounds as there is a strong electrostatic repulsion between them [7]. Furthermore, the potential separation problem still limits the application of graphene and GO. Therefore, one possible route to improve these properties for applications is to combine graphene materials with other particles to form nanocomposites, which has been proven to be an effective and feasible method to avoid the aggregation of individual graphene sheets and nanoparticles, thus overcoming the separation problem [19–21].

Due to their advantages such as environmental friendliness, hydrophilicity, chemical resistance, high strength, and low cost [22–24], SiO_2 nanoparticles are undoubtedly a good candidate to decorate graphene materials to overcome the shortage of individual sheets. Thus, SiO_2/RGO nanocomposites were selected as the promising adsorbents in this study.

In recent years, SiO_2/RGO nanocomposites have been fabricated via different methods. For instance, Hao et al. [25] reported the preparation of SiO_2/graphene composites through a two-step reaction, including the synthesis of SiO_2/GO and the reduction of GO. Zhou and Shi [26] studied a more simplified hydrothermal synthesis of SiO_2-graphene

hybrid but without investigation of application. Liu et al. [27] developed a simple method to construct PEI@SiO_2@rGO composites to remove Hg^{2+} and dyes from contaminated water. Through typical sol-gel technique, Zeng et al. [28] synthesized SiO_2-coated GO sheets in a water-alcohol-ammonia mixture to prepare SiO_2-GO-MIPs sensor. Li et al. [29] prepared SiO_2/RGO nanosheet composites through a modified sol-gel process with $NH_2NH_2{\cdot}H_2O$ as reductant. Overall, most synthesis processes used in the abovementioned previous studies are relatively complex, including at least two main steps, or reduced by adding reductants. And some synthesis methods with low adsorption efficiencies are rarely used in the actual treatment process.

Herein, we report an efficient one-step hydrothermal method to fabricate SiO_2/RGO nanocomposites through the reaction of silica sol and GO in a sealed stainless steel reactor with PTFE lining. This facile fabrication procedure combines the reduction of GO and the preparation of SiO_2/RGO nanocomposites in one step. The adsorption performance of SiO_2/RGO nanocomposites for hexavalent chromium (Cr(VI)) was investigated in aqueous solution. It is well known that Cr(VI) is mainly caused by dragout, chromate passivation solutions, and rinsing of plated articles, which has high toxicity and high mobility in water and causes great harm to the environment and human health. Currently, adsorption method has been widely used for Cr(VI) removal [30–32]. However, the low efficiency and complicated producing process of these adsorbents limits its application [33, 34]. Therefore, it is necessary to explore more suitable adsorbents with high efficiency, facile synthesis process, and low cost for Cr(VI) removal. In this study, a new method has been developed to synthesize SiO_2/RGO nanocomposite by one-step process. The obtained nanocomposites with large specific surface area (676 m^2/g) and unique hierarchical micro-mesoporous structure show superior performance in adsorption of Cr(VI). The hierarchical micro-mesoporous SiO_2/RGO nanocomposites present great potential in the fields of environmental remediation.

2. Experimental

2.1. Materials. Tetraethyl orthosilicate (TEOS, 28%), nitric acid (65%), diphenylcarbohydrazide, hydrochloric acid (36~38%), potassium permanganate, hydrogen peroxide, and phosphoric acid (>85%) (Sinophare Chemical Reagent Co., Ltd.) were all of analytical grade and potassium dichromate (Shanghai Chemical Reagent Co., Ltd.) and natural flake graphite (Sinophare Chemical Reagent Co., Ltd.) with particle size below 30 μm were of chemical grade. All reagents were obtained from commercial sources and used without further purification.

2.2. Synthesis of SiO_2/RGO Nanocomposites. Through a one-step method, SiO_2/RGO nanocomposite samples were synthesized by hydrolyzing tetraethyl orthosilicate (TEOS) directly in a GO aqueous dispersion, which was prepared according to the Hummers method through the oxidation of natural flake graphite [35]. The synthesized GO suspension (9.0 g, 1 wt.%) was diluted with 100 mL deionized water and then was ultrasonicated for 15 min. The pH of the solution was adjusted to 1.0 with 0.1 M HNO_3. TEOS solution with different volume (1 mL, 2 mL, and 3 mL) was then slowly added to the above suspension with magnetic stirring at 40°C. Such obtained mixture with different mass ratio of GO and SiO_2 (1 : 3, 1 : 6, and 1 : 9) underwent hydrothermal reaction in a 200 mL cylindrical sealed stainless steel reactor with polytetrafluoroethylene (PTFE) lining at 120°C for 12 h. During the process of hydrothermal reaction, GO was reduced while a portion of functional oxygen groups was removed to recover the densely packed benzene-ring structure partially. Meanwhile, along with the process of hydrolysis of TEOS, different forms of silica were loaded on the surface of GO sheets through covalent bond linkage [36]. As a result, the amorphous SiO_2 particles were incorporated onto the surface of the RGO films. Finally, the synthesized composite samples were collected through centrifuge for 5 min at 4000 rpm and washed with deionized water until neutral. The samples were then dried overnight at 60°C in air. The samples were as assigned as SiO_2/RGO-1, SiO_2/RGO-2, and SiO_2/RGO-3 corresponding to GO and SiO_2 mass ratio of 1 : 3, 1 : 6, and 1 : 9, respectively. For comparison, the pure SiO_2 was obtained by the hydrolysis of TEOS under the same procedure of SiO_2/RGO preparation but without adding GO.

2.3. Cr(VI) Adsorption and Method of Analysis. The adsorption experiments were carried out in a 200 mL glass jacketed batch reactor operated at 180 rpm rotating speed. A certain amount of SiO_2/RGO nanocomposites were dispersed into the solution, and the aqueous solutions of Cr(VI) were adjusted to different concentrations using $K_2Cr_2O_7$. The pH was controlled using 0.5 M HCl and 0.5 M NaOH and the temperature was regulated by super-thermostatic water bath. The SiO_2/RGO nanocomposites were separated by centrifugation and the concentration of Cr(VI) at different time intervals in the batch reactor was determined using 1,5-diphenylcarbohydrazide (DPC) spectrophotometry method and the measuring wavelength is 540 nm. The adsorption efficiency (E, %) was calculated by the following equation:

$$E = \frac{100\% \left(C_0 - C_t\right)}{C_0}, \quad (1)$$

where C_0 and C_t (mg/L) are the concentrations of Cr(VI) at initial time and the time of sampling, respectively. All experiments were repeated twice to ensure the reproducibility.

2.4. Characterization of the SiO_2/RGO Nanocomposites. The morphology of GO and SiO_2/RGO nanocomposite was investigated by a transmission electron microscopy (TEM, JEM-2100, JEOL). The functional groups of the samples were analyzed by Fourier transform infrared (FT-IR) spectroscopy using Nicolet Nexus 470 FT-IR Spectrometer in the range of 400~4000 cm^{-1}. The X-ray diffraction (XRD) patterns of the synthesized samples were obtained using a D8 Advance diffractometer (Bruker, Germany) with Cu K radiation (0.15418 nm) and scanning rate 5°/min. The samples were also studied by a TG-DSC (Thermogravimetric and Differential Scanning Calorimetric Method) in oxygen at heating

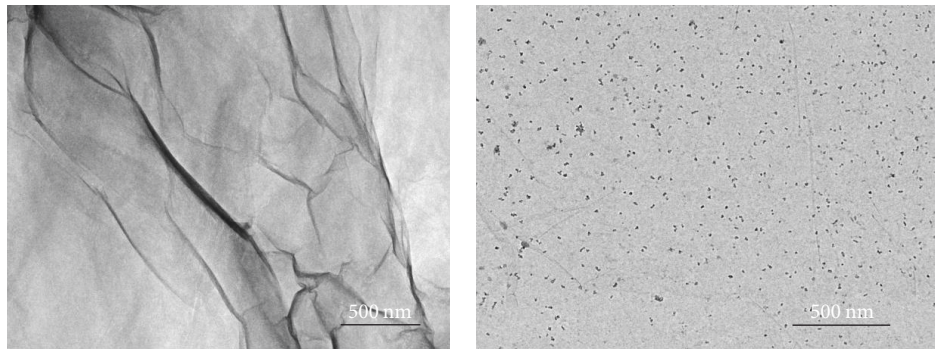

(a) (b)

Figure 1: TEM images of GO (a) and of SiO_2/RGO-2 nanocomposites (b).

rate of 10°C/min. N_2 adsorption-desorption isotherms were measured using a Quantachrome Autosorb-iQ-MP (USA) analyzer at −196°C with a relative pressure ranging from 0.0112 to 0.9948. The specific surface area was calculated by a Brunauer Emmett Teller (BET) model.

3. Results and Discussion

3.1. Material Characterization. The morphologies of GO nanosheets and SiO_2/RGO-2 nanocomposites samples were fully analyzed by TEM in Figure 1. Figure 1(a) shows the TEM images of the GO membrane with a lateral size of several micrometers. The wrinkled morphology was compatible with the mechanisms of the stability of 2D membranes that had intrinsic ripples owing to thermal fluctuations [37]. As shown in Figure 1(b), SiO_2 nanoparticles were uniformly distributed on the surface of the corrugated platelet of RGO, which was obtained from the reduction of GO through hydrothermal reaction, consistent with the FT-IR results. Compared with the image of GO in Figure 1(a), restacking was much less due to the loading of SiO_2 nanoparticles. It is obvious that nanoparticles of SiO_2 have been loaded uniformly onto the RGO membrane.

FT-IR spectra of GO, RGO, SiO_2, and SiO_2/RGO-2 are shown in Figure 2. The following functional groups are identified in the GO sample in Figure 2(a): a broad and strong peak appearing at 3386 cm^{-1} assigned to O-H stretching vibration; the C=O stretching vibration of -COOH groups at 1732 cm^{-1}; the O-H bending vibration and sp^2 C=C stretching of skeletal ring at around 1624 cm^{-1}; the adsorption at 1215 cm^{-1} and 1172 cm^{-1} attributed to C-O vibration and C-O-C vibration, respectively. The peak at 864 cm^{-1} and 590 cm^{-1} is possibly attributed to C-H bonds out-plane bending vibration. It is obvious that the well-oxidized GO has been synthesized and -OH, -COOH, -CHO, and -C-O-C- functional groups existed in GO sample [38, 39]. After hydrothermal treatment, as shown in Figure 2(b), the peak at 1732 cm^{-1} (C=O stretching vibration of -COOH groups) disappears completely and other characteristic peaks at 1630 cm^{-1} (C=C in phenol ring) and 1150 cm^{-1} (C-O-C vibration) become weak, confirming the reduction of GO. Meanwhile, a new band displays at 1439 cm^{-1} which is contributed from the C-H bending vibrations of the reduced graphene lattice. In Figure 2(c), the characteristic peaks of SiO_2 are as follows: the broad adsorption at 3454 cm^{-1} is attributed to the stretching vibration of -OH in structural water, and the peak at 1636 cm^{-1} is related to the H-O-H bending vibration of residual water molecules [40, 41]. Similar to the spectra of RGO, several peaks assigned to oxygen functional groups at 3386, 1732, 1630, and 1150 cm^{-1} become weak or disappear, which implies that GO was partially reduced. In Figure 2(d), the sharp adsorption at 1101 cm^{-1} is due to Si-O-C or Si-O-Si stretching vibration and Si-OH bending vibration lies at 968 cm^{-1} [42]. The peaks at 796 cm^{-1} and 471 cm^{-1} are assigned to the stretching and bending vibrations of Si-O bonds, respectively. It is therefore quite certain that SiO_2 nanoparticles existed in the nanocomposites synthesized in this study. Furthermore, the fact that the spectra of RGO become weak or unclear in Figure 2(d) is not only due to the partial reduction of GO, but also due to the reaction between oxygen functional groups and Si-OH, which can be indirectly proved by the formation of a covalent bonding Si-O-C between RGO sheets and SiO_2 nanoparticles [43]. Based on the above analysis, it can be concluded that SiO_2 nanoparticles are well-dispersed on the surface of RGO sheets.

Figure 3 shows the XRD patterns of graphite, GO, RGO, SiO_2, and SiO_2/RGO-2 nanocomposites samples. It can be seen that graphite and GO samples exhibit two sharp and intense peaks centered at 26.5° (Figure 3(a)) and 9.4° (Figure 3(b)), respectively. Both of them are the typical (002) diffraction peaks consistent with previous studies [8, 22]. According to Bragg equation ($2d \sin\theta = n\lambda$), the corresponding lattice parameter of GO is determined to be 0.94 nm, which is larger than that of graphite (0.334 nm), due to the existence of oxygen functional groups. After hydrothermal reduction, GO nanosheets were partially reduced to RGO nanosheets. This is evidenced by the appearance of the (002) diffraction peak at 24.9° and the (100) diffraction peak at 43.0° (Figure 3(c)). The broad diffraction peak in the range of 15~35° and centered at 21.9° (Figure 3(d)) is assigned as amorphous SiO_2 obtained by the hydrothermal method. In Figure 3(e), the diffraction pattern of SiO_2/RGO-2 is similar to that of amorphous SiO_2, but the center of the newly obtuse

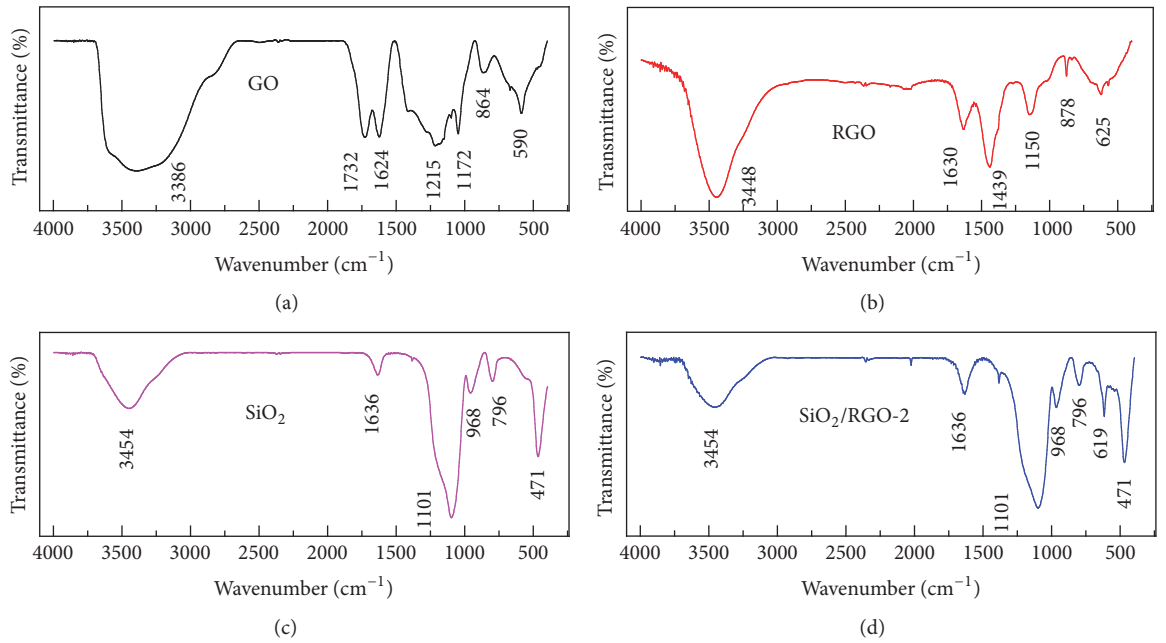

Figure 2: FT-IR spectra of GO, RGO, and SiO_2/RGO-2 nanocomposite samples.

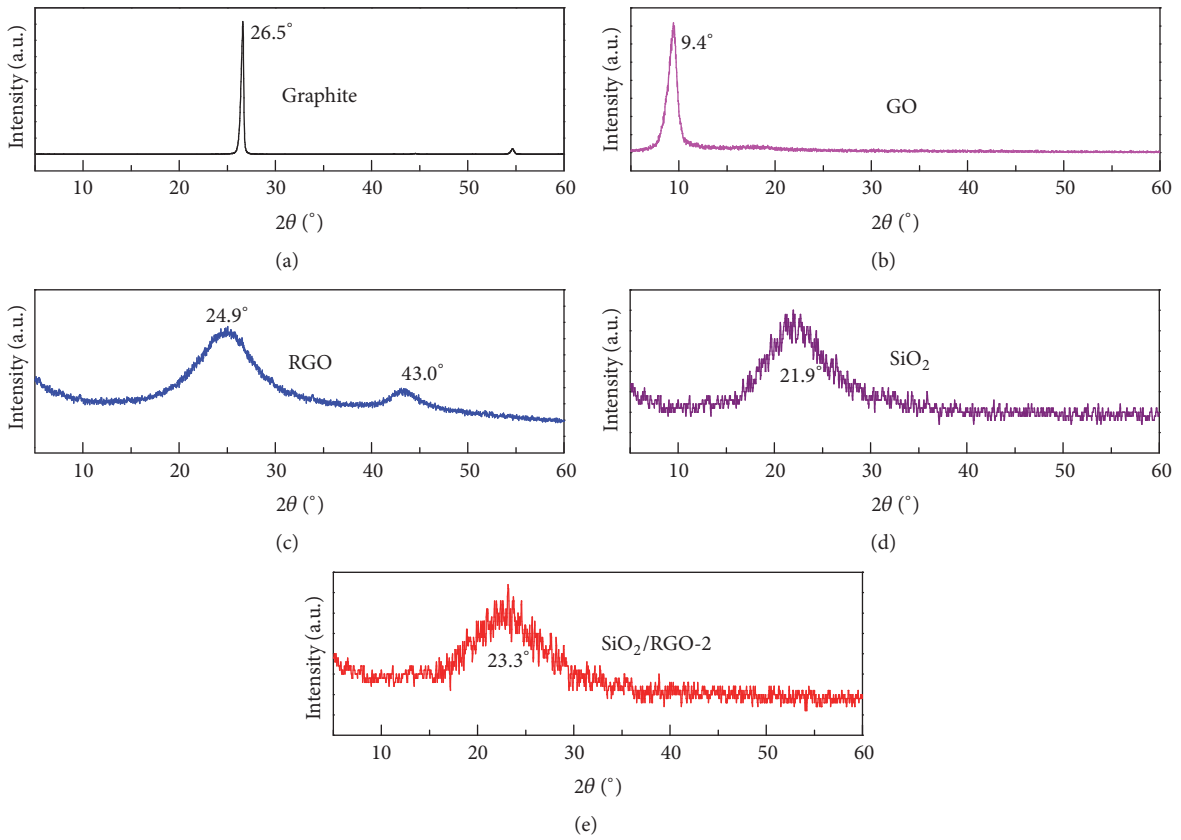

Figure 3: XRD patterns of graphite, GO, RGO, SiO_2, and SiO_2/RGO-2 nanocomposites.

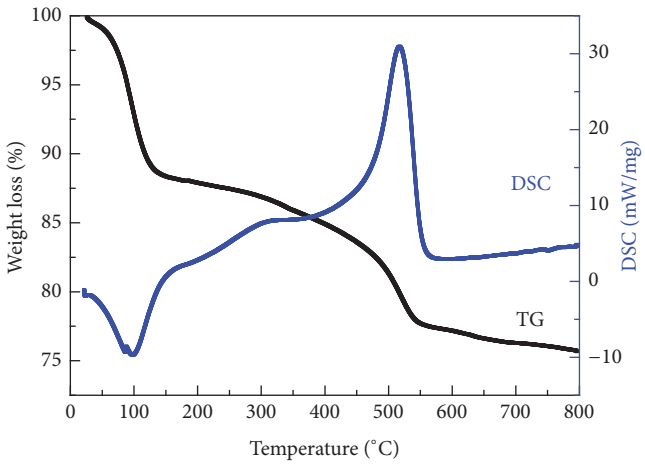

Figure 4: TG-DSC profiles of the as-prepared SiO_2/RGO-2 nanocomposites.

peak has shifted to 23.3° because of the influence of RGO with lattice parameter of 0.380 nm, which is slightly bigger than that of graphite, due to remaining oxygen functional groups. Moreover, the (100) diffraction peak at 43.0° disappears due to the coverage of SiO_2 nanoparticles.

Figure 4 shows TG-DSC profiles of the as-prepared SiO_2/RGO-2 nanocomposite sample. It can be seen that the weight loss of the SiO_2/RGO-2 nanocomposite is divided into three stages and the curve of DSC exhibits two major distinct peaks. The first low-temperature weight loss under 100°C is primarily due to the evaporation of adsorbed free water and water held on the surface by hydrogen bonding, which is an endothermic process as illustrated by the endothermic peak of DSC curve. Weight loss in the range of 100–450°C is attributed to the decomposition and removal of oxygen functionalities including hydroxyl, carboxylic, and epoxide groups [40]. And the weight loss from 450 to 550°C is likely attributed to the decomposition of the carbon skeleton of RGO, corresponding to the obvious exothermic peak of DSC curve. Further weight loss above 550°C is minimal and the remaining mass is SiO_2 particles [42, 44]. The content of SiO_2 loaded on RGO in the nanocomposite is 74.68%.

The N_2 adsorption-desorption isotherms and pore size distributions of SiO_2/RGO nanocomposites are presented in Figure 5 and Table 1. For SiO_2/RGO-1, it has hierarchical micro-mesoporous structure including 63% micropores and 37% mesopores as listed in Table 1, but a typical type II isotherm with a small hysteresis phenomenon corresponds to a relatively low porosity material in agreement with the lower specific surface area (514 m^2/g). For SiO_2/RGO-3, a typical type IV isotherm with an obvious hysteresis phenomenon indicates the existence of abundant mesopores (658 m^2/g) and the ratio of mesopores (V_{mes}/V_t) reaches up to 98.09% (Table 1). In comparison, the N_2 adsorption-desorption isotherms of SiO_2/RGO-2 exhibit combined characteristics of type II and type IV, which shows a noticeable nitrogen adsorption increment in the low pressure region from 0.0 to 0.5 P/P_0 (Figure 5(a)) followed by a gradual increase with increasing the relative pressure and displays a long hysteresis at almost the whole range of relative pressure [25]. The results suggest that SiO_2/RGO-2 possesses rich microporous and mesoporous structure, which is also proved by the data of Table 1 (especially V_{mes}/V_t = 65.18%) and shown by the pore distribution curve of Figure 5(b). Meanwhile, the long hysteresis loop belongs to typical H4 model, suggesting that the pores in the composites mainly consisted of slit apertures formed by the stack of layered materials, different from the only packing of particles. It can be concluded that the adsorption mainly takes place on the surface and the interlayer of plate-like nanocomposites [26, 45].

Furthermore, the increase of the proportion of SiO_2 will reduce the cost of the production of SiO_2/RGO nanocomposites, but the excessive SiO_2 led to unreasonable pore structure, as illustrated in Table 1. Although the BET surface area of SiO_2/RGO-3 increased to 691 m^2/g, the surface area of micropores decreased dramatically to 33 m^2/g, which undermines the adsorption of Cr(VI) ions. In comparison, the BET surface area and pore volume calculated by Barret-Joyner-Halenda (BJH) method of SiO_2/RGO-2 were 676 m^2/g and 0.4265 cm^3/g, respectively. It has not only higher surface area than SiO_2/RGO-1 but also more reasonable hierarchical micro-mesoporous structure than SiO_2/RGO-3, including mesoporous surface area 371 m^2/g and microporous surface area 305 m^2/g. Mesopores not only provide active sites but also facilitate ions diffusion and enhance micropores supply higher adsorption sites. This hierarchical micro-mesoporous structure is beneficial to the adsorption of Cr(VI) ions in wastewater. From the above analysis, Due to the hierarchical micro-mesoporous structure and the high surface area, SiO_2/RGO-2 nanocomposite has greater potential for Cr(VI) adsorption.

3.2. Cr(VI) Adsorption Performance. Using Cr(VI) ions solutions to simulate wastewater, the adsorption performance of the as-prepared SiO_2/RGO samples was evaluated through the removal efficiency of Cr(VI) ions. The adsorption activity was examined under different conditions. 100 mL initial solution containing Cr(VI) with the concentration of 10 mg/L was charged into the jacketed batch reactor operated at 20°C. Different samples (100 mg) were dispersed in the solution by stirring at 200 rpm and the pH = 2. The adsorption curves were obtained through UV-vis spectrophotometer by measuring the absorbance of Cr(VI) in the samples gathered at different time intervals. The changes of adsorption efficiencies are given in Figure 6.

The adsorption performance of SiO_2/RGO nanocomposites was assessed. As shown in Figure 6(a), the results suggest that the adsorption efficiency of all SiO_2/RGO nanocomposites (>90%) was higher than that of the pure SiO_2 nanoparticles (26.5%) and pure RGO (56.7%) with same dosage. Obviously, the composite was not just a physical mixture of two substances but a new nanocomposite material. The prevention of the restacking of sheets and the aggregation of SiO_2 nanoparticles contributed to the improved Cr(VI) removal efficiency.

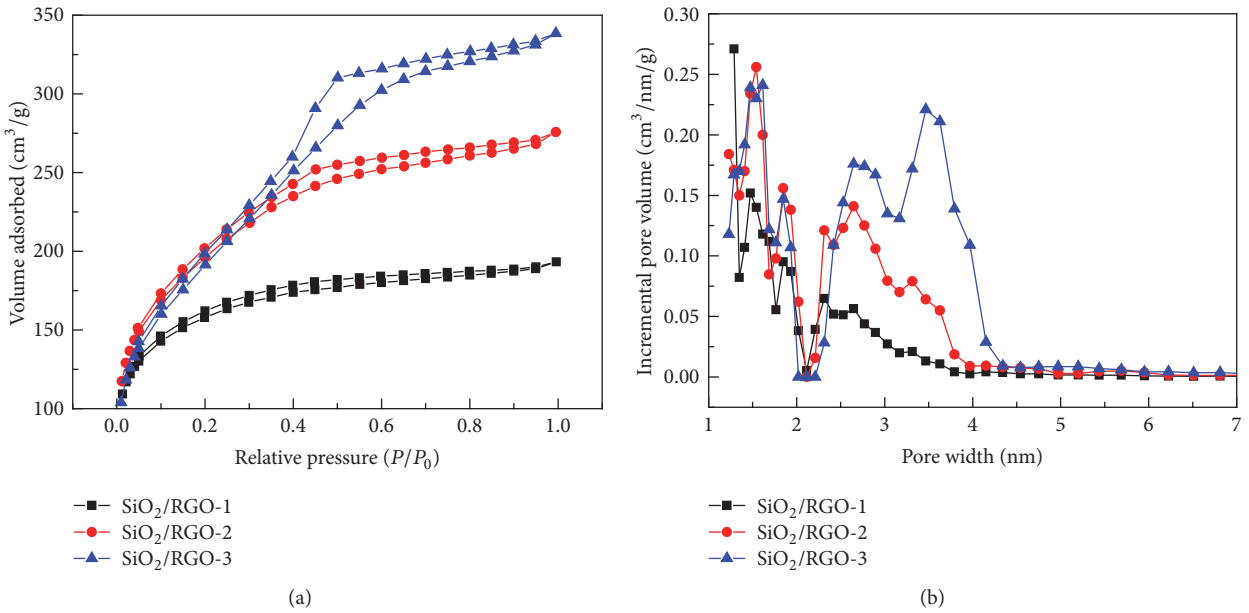

Figure 5: Nitrogen adsorption-desorption isotherms (a) and pore size distribution curve (b) of SiO_2/RGO nanocomposites.

Table 1: Pore structure parameters of different SiO_2/RGO nanocomposites.

Sample	S_{BET} ($m^2 \cdot g^{-1}$)	S_{mic} ($m^2 \cdot g^{-1}$)	S_{mes} ($m^2 \cdot g^{-1}$)	V_t ($cm^3 \cdot g^{-1}$)	V_{mic} ($cm^3 \cdot g^{-1}$)	V_{mes} ($cm^3 \cdot g^{-1}$)	V_{mes}/V_t (%)
SiO_2/RGO-1	514	138	376	0.2989	0.1880	0.1109	37.10
SiO_2/RGO-2	676	305	371	0.4265	0.1480	0.2780	65.18
SiO_2/RGO-3	691	33	658	0.5236	0.0100	0.5136	98.09

S_{BET}, BET specific surface area; S_{mic}, micropore surface area; S_{mes}, mesopore surface area; V_t, total pore volume; V_{mic}, micropore volume; V_{mes}, mesopore volume.

Meanwhile, the curves in Figure 6(a) showed that the adsorbent of SiO_2/RGO-2 exhibited better adsorption efficiency than that of SiO_2/RGO-1 and SiO_2/RGO-3 samples. The uptake of Cr(VI) by SiO_2/RGO-2 adsorbents increased dramatically in the first 10 min and reached the equilibrium in 60 min with a adsorption efficiency of 98.8%, which demonstrated superior adsorption rate and efficiency [46, 47]. In addition, the Cr(VI) concentration after treatment with SiO_2/RGO-2 adsorbent drops below 12 μg/L, which completely meets the standards for drinking set by the World Health Organization [48]. This phenomenon was attributed to higher specific surface area than SiO_2/RGO-1 and more reasonable hierarchical micro-mesoporous structure than SiO_2/RGO-3, which was consistent with the analysis of N_2 adsorption-desorption. Furthermore, as shown in Figure 6(b), the stability of SiO_2/RGO-2 nanocomposites was studied by comparing the adsorption performance between the fresh sample (SiO_2/RGO-2 (new)) and the aged sample that was kept for six months after preparation (SiO_2/RGO-2 (aged)). The SiO_2/RGO-2 (aged) adsorbent had the adsorption efficiency with 98.6%, nearly the same as that of the freshly prepared adsorbent samples. So it is believed that the SiO_2/RGO nanocomposite has more superior stability than the pure SiO_2 nanoparticles and pure RGO sheets.

3.3. Mechanism of SiO_2/RGO Formation and Cr(VI) Adsorption. The composites of SiO_2/RGO were successfully synthesized through one-step hydrothermal method. The recombined process was illustrated by the schematic of Figure 9 step A. At the beginning, using TEOS as silica source SiO_2 nanoparticles formed through hydrolysis and dehydrate process [49]. Simultaneously, superheated H_2O promotes acid-catalyzed reaction of organic compounds because of a sufficiently high H+ concentration compared to normal liquid phase [50, 51]. The H^+-catalyzed dehydration could make GO be reduced partially [52, 53] and make part of oxygen functional groups break away from the skeleton [54]. At last, the SiO_2 nanoparticles were anchored onto the surface of RGO owing to electrostatic interactions and covalent reaction. Similar to graphene sheets, the surface charge containing delocalized electrons was regarded as negative [55]. In contrast, the zeta potential of SiO_2 nanoparticles was positive when pH value was less than 3 (Figure 7). Therefore, the RGO sheets possessed the ability to attach SiO_2 nanoparticles through electrostatic interaction. Additionally, silicon hydroxyls easily interact with oxygen functional groups (e.g., -COOH, -OH) through covalent reaction (Figure 9 step A). During this process, RGO sheets were further unfolded and

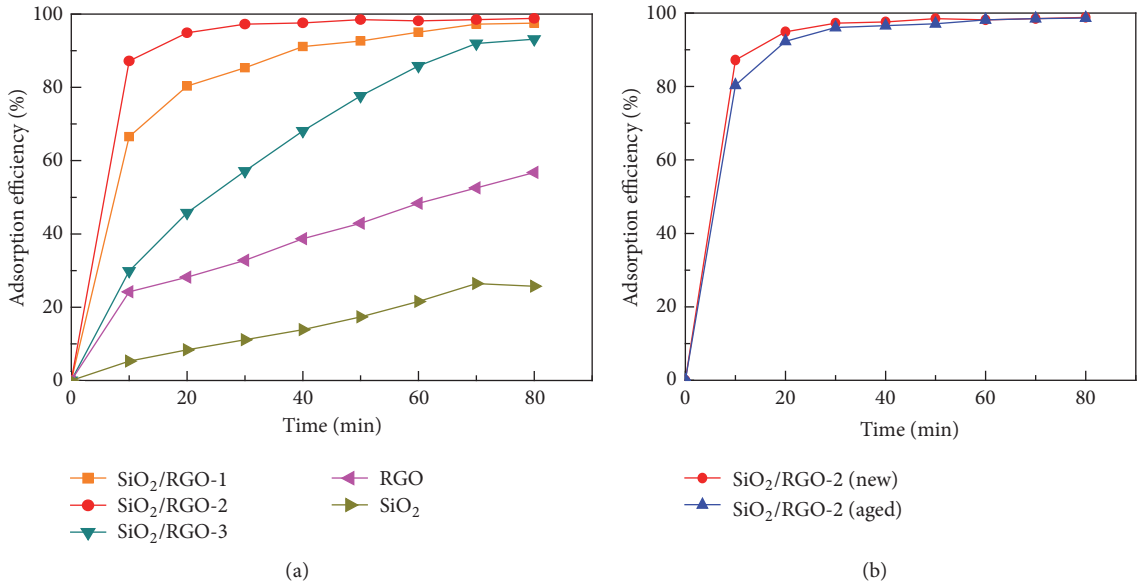

FIGURE 6: Adsorption efficiency curves of RGO, SiO_2 nanoparticles and SiO_2/RGO nanocomposites (a) and adsorption efficiency curves of SiO_2/RGO (new) and SiO_2/RGO (aged) (b).

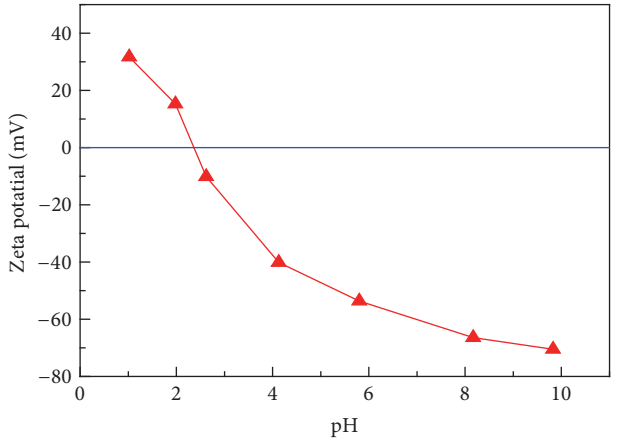

FIGURE 7: Relationship between pH and zeta potential of SiO_2 nanoparticles.

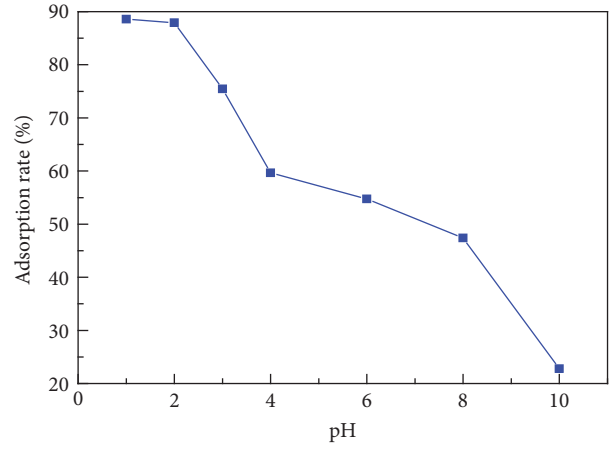

FIGURE 8: Effects of pH on the Cr(VI) removal efficiency.

improved the stability because of the electrostatic repulsion among SiO_2 nanoparticles.

The adsorption mechanism was schematically illustrated in step B and step C of Figure 9. The Cr(VI) adsorption capacity of SiO_2/RGO was closely related to pH value due to its influence on the surface properties of the adsorbent and different ionic forms of the chromium solutions [56]. Chromium existed in different oxidation states and the stability of these forms is dependent upon the pH of the system [57]. The equilibrium between different ionic chromium species can be described as follows:

$$H_2CrO_4 \Longleftrightarrow H^+ + HCrO_4^- \quad (2)$$

$$HCrO_4^- \Longleftrightarrow H^+ + CrO_4^{2-} \quad (3)$$

$$2HCrO_4^- \Longleftrightarrow Cr_2O_7^{2-} + H_2O \quad (4)$$

With increasing pH value, the chromium ions were converted from $HCrO_4^-$ into CrO_4^{2-} and $Cr_2O_7^{2-}$. The effect of pH on adsorption of Cr(VI) was illustrated in Figure 8. It is obvious that the adsorption efficiency of Cr(VI) decreased sharply as the pH increased from 1.0 to 8.0, showing the strong dependence of Cr(VI) removal performance on the system's pH. The highest efficiency with ~92% Cr(VI) removal was achieved in the pH of 1~2, in which adsorption capacity increased to the maximum value without apparent change of chromium form, mainly $HCrO_4^-$. It is therefore

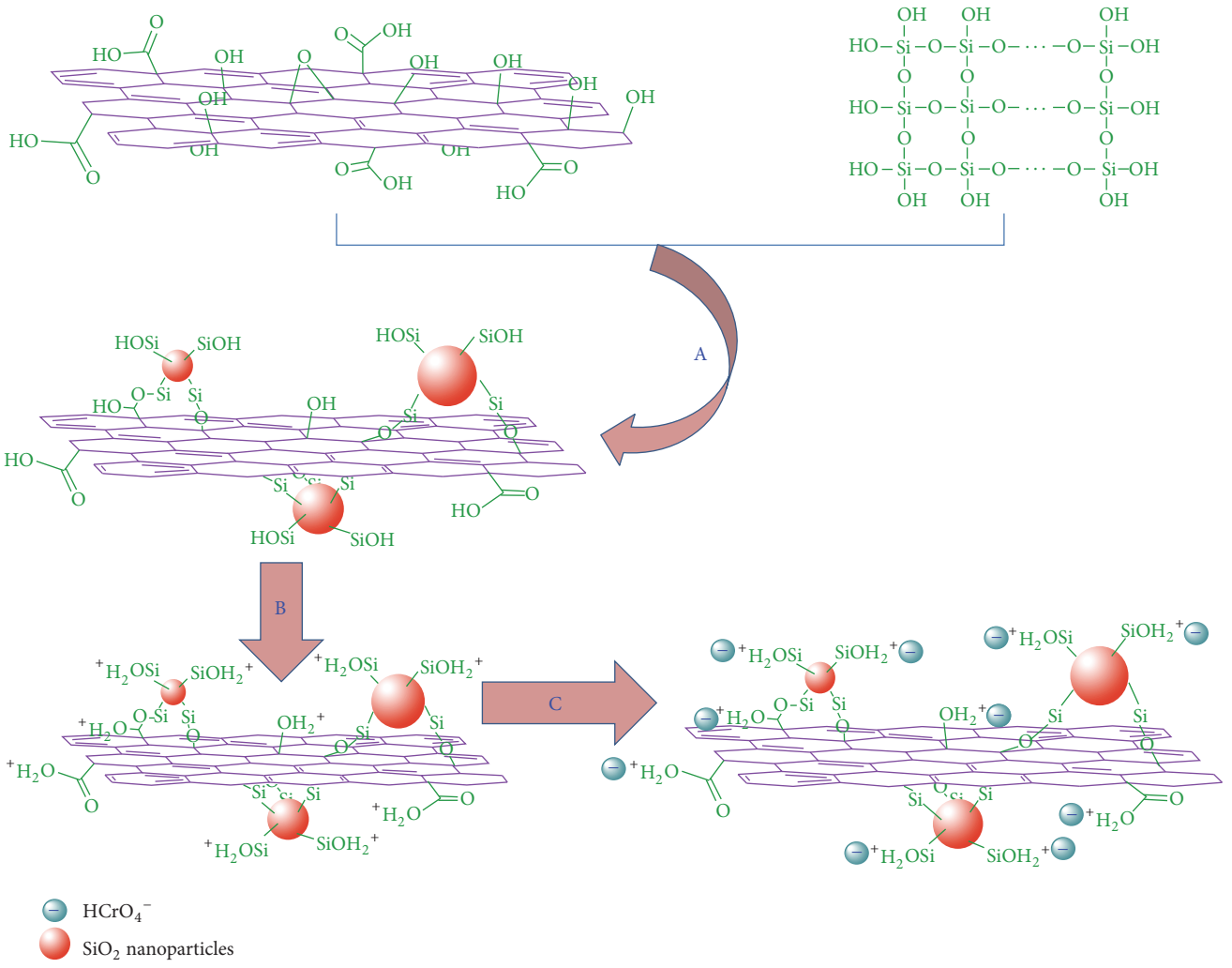

Figure 9: Schematic pathway of the recombination and adsorption mechanisms.

obvious that the low pH leads to an increase in the concentration of H^+ ions [58]. In highly acidic media, the adsorbent surfaces might be highly protonated to positive charges [59], as shown in Figure 9 step B. The positive charges represent the protonation of -OH [60]. Therefore, as illustrated in Figure 9 step C, strong electrostatic attraction exists between the positively charged nanocomposites surface and $HCrO_4^-$, which was the dominant form of Cr(VI) at pH less than 2.0. Unlike CrO_4^{2-}, $HCrO_4^-$ only need one adsorption site to facilitate them, leading to high adsorption efficiency at pH less than 2.0.

4. Conclusions

A low cost SiO_2/RGO nanocomposite adsorbent with hierarchical micro-mesoporous structure was successfully synthesized by means of a feasible one-step hydrothermal method. The adsorbent can remove Cr(VI) ions from aqueous solution effectively. SiO_2 nanoparticles (ca.10 nm) were uniformly distributed on the membrane of RGO, which not only improved the stability of composites owing to preventing the restacking of RGO sheets, but also made the separation easier due to the relatively high intensity of SiO_2. The adsorption efficiency of Cr(VI) ions reached 98.8%, and the adsorption reached equilibrium in 30 min. The results suggest that SiO_2/RGO nanocomposites adsorbent is suitable for effective and rapid removal of Cr(VI) ions from wastewater.

Conflicts of Interest

The authors declare that there are no conflicts of interest regarding the publication of this paper.

Acknowledgments

This work was supported by the National Natural Science Foundation of China (51404097, 51404098, 51472075, and U1361119), International Science and Technology Cooperation Project of Henan province (152102410047), and National Science Research Program of Henan Provincial Education Department (no. 2011B440006).

References

[1] K. S. Novoselov, A. K. Geim, S. V. Morozov et al., "Electric field in atomically thin carbon films," *Science*, vol. 306, no. 5696, pp. 666–669, 2004.

[2] K. S. Novoselov, D. Jiang, F. Schedin et al., "Two-dimensional atomic crystals," *Proceedings of the National Academy of Sciences of the United States of America*, vol. 102, no. 30, pp. 10451–10453, 2005.

[3] A. A. Balandin, S. Ghosh, W. Bao et al., "Superior thermal conductivity of single-layer graphene," *Nano Letters*, vol. 8, pp. 902–907, 2008.

[4] T. Stauber, N. M. R. Peres, and A. K. Geim, "Optical conductivity of graphene in the visible region of the spectrum," *Physical Review B - Condensed Matter and Materials Physics*, vol. 78, no. 8, Article ID 085432, 2008.

[5] Y. Cao and X. Li, "Adsorption of graphene for the removal of inorganic pollutants in water purification: a review," *Adsorption*, vol. 20, no. 5-6, pp. 713–727, 2014.

[6] A. M. Jastrzebska, P. Kurtycz, and A. R. Olszyna, "Recent advances in graphene family materials toxicity investigations," *Journal of Nanoparticle Research*, vol. 14, no. 12, p. 1320, 2012.

[7] S. Chowdhury and R. Balasubramanian, "Recent advances in the use of graphene-family nanoadsorbents for removal of toxic pollutants from wastewater," *Advances in Colloid and Interface Science*, vol. 204, pp. 35–56, 2014.

[8] A. Peigney, C. Laurent, E. Flahaut, R. R. Bacsa, and A. Rousset, "Specific surface area of carbon nanotubes and bundles of carbon nanotubes," *Carbon*, vol. 39, no. 4, pp. 507–514, 2001.

[9] A. K. Geim and K. S. Novoselov, "The rise of graphene," *Nature Materials*, vol. 6, no. 3, pp. 183–191, 2007.

[10] N. Ferralis, "Probing mechanical properties of graphene with Raman spectroscopy," *Journal of Materials Science*, vol. 45, no. 19, pp. 5135–5149, 2010.

[11] A. K. Farquhar, H. M. Dykstra, M. R. Waterland, A. J. Downard, and P. A. Brooksby, "Spontaneous modification of free-floating few-layer graphene by aryldiazonium ions: electrochemistry, atomic force microscopy, and infrared spectroscopy from grafted films," *Journal of Physical Chemistry C*, vol. 120, no. 14, pp. 7543–7552, 2016.

[12] G. K. Raghu, M. T. Hanumantharaju, and N. Siddappa, "Electrochemically assisted synthesis of graphene-anthraquinone composite: sensing platform for ascorbic acid," *International Journal of Innovative Research and Development*, vol. 5, no. 11, 2016.

[13] D. D. Nguyen, N.-H. Tai, S.-B. Lee, and W.-S. Kuo, "Superhydrophobic and superoleophilic properties of graphene-based sponges fabricated using a facile dip coating method," *Energy and Environmental Science*, vol. 5, no. 7, pp. 7908–7912, 2012.

[14] J. Tong, H.-X. Huang, and M. Wu, "Facile green fabrication of well dispersed poly(vinylidene fluoride)/graphene oxide nanocomposites with improved properties," *Composites Science and Technology*, vol. 129, pp. 183–190, 2016.

[15] M. Z. Iqbal, A. A. Abdala, V. Mittal, S. Seifert, A. M. Herring, and M. W. Liberatore, "Processable conductive graphene/polyethylene nanocomposites: Effects of graphene dispersion and polyethylene blending with oxidized polyethylene on rheology and microstructure," *Polymer (United Kingdom)*, vol. 98, pp. 143–155, 2016.

[16] A. Lerf, H. He, M. Forster, and J. Klinowski, "Structure of graphite oxide revisited," *The Journal of Physical Chemistry B*, vol. 102, no. 23, pp. 4477–4482, 1998.

[17] D. W. Lee, V. L. De Los Santos, J. W. Seo et al., "The structure of graphite oxide: investigation of its surface chemical groups," *Journal of Physical Chemistry B*, vol. 114, no. 17, pp. 5723–5728, 2010.

[18] R. Cruz-Silva, M. Endo, and M. Terrones, "Graphene oxide films, fibers, and membranes," *Nanotechnology Reviews*, vol. 5, no. 4, pp. 377–391, 2016.

[19] Y. Gong, C. Zou, Y. Yao et al., "A facile approach to synthesize rose-like ZnO/reduced graphene oxide composite: fluorescence and photocatalytic properties," *Journal of Materials Science*, vol. 49, no. 16, pp. 5658–5666, 2014.

[20] H. Song, L. Zhang, C. He, Y. Qu, Y. Tian, and Y. Lv, "Graphene sheets decorated with SnO2 nanoparticles: In situ synthesis and highly efficient materials for cataluminescence gas sensors," *Journal of Materials Chemistry*, vol. 21, no. 16, pp. 5972–5977, 2011.

[21] H. Liu, L. Deng, Z. Zhang, J. Guan, Y. Yang, and Z. Zhu, "One-step in-situ hydrothermal synthesis of SnS_2/reduced graphene oxide nanocomposites with high performance in visible light-driven photocatalytic reduction of aqueous Cr(VI)," *Journal of Materials Science*, vol. 50, no. 8, pp. 3207–3211, 2015.

[22] F.-Q. Tang, Z. Xiao, J.-A. Tang, and L. Jiang, "The effect of SiO_2 particles upon stabilization of foam," *Journal of Colloid And Interface Science*, vol. 131, no. 2, pp. 498–502, 1989.

[23] Y. Masuda, M. Itoh, T. Yonezawa, and K. Koumoto, "Low-dimensional arrangement of SiO2 particles," *Langmuir*, vol. 18, no. 10, pp. 4155–4159, 2002.

[24] S. Musić, N. Filipović-Vinceković, and L. Sekovanić, "Precipitation of amorphous SiO_2 particles and their properties," *Brazilian Journal of Chemical Engineering*, vol. 28, no. 1, pp. 89–94, 2011.

[25] L. Hao, H. Song, L. Zhang, X. Wan, Y. Tang, and Y. Lv, "SiO_2/graphene composite for highly selective adsorption of Pb(II) ion," *Journal of Colloid and Interface Science*, vol. 369, no. 1, pp. 381–387, 2012.

[26] X. Zhou and T. Shi, "One-pot hydrothermal synthesis of a mesoporous SiO_2-graphene hybrid with tunable surface area and pore size," *Applied Surface Science*, vol. 259, pp. 566–573, 2012.

[27] X. Liu, Y. Gao, H. Luo, and R. Jin, "Synergistically constructed polyamine/nanosilica/graphene composites: Preparation, features and removal of Hg^{2+} and dyes from contaminated water," *RSC Advances*, vol. 4, no. 19, pp. 9594–9601, 2014.

[28] Y. B. Zeng, Y. Zhou, L. Kong, T. Zhou, and G. Shi, "A novel composite of SiO_2-coated graphene oxide and molecularly imprinted polymers for electrochemical sensing dopamine," *Biosensors and Bioelectronics*, vol. 45, no. 1, pp. 25–33, 2013.

[29] W. Li, W. Liu, H. Wang, and W. Lu, "Preparation of silica/reduced graphene oxide nanosheet composites for removal of organic contaminants from water," *Journal of Nanoscience and Nanotechnology*, vol. 16, no. 6, pp. 5734–5739, 2016.

[30] J. Qu, D. Chen, N. Li et al., "Coral-inspired nanoscale design of porous SnS 2 for photocatalytic reduction and removal of aqueous Cr (VI)," *Applied Catalysis B: Environmental*, vol. 207, pp. 404–411, 2017.

[31] Y. Zhao, W. Chang, Z. Huang et al., "Enhanced removal of toxic Cr(VI) in tannery wastewater by photoelectrocatalysis with synthetic TiO_2 hollow spheres," *Applied Surface Science*, vol. 405, pp. 102–110, 2017.

[32] Z. Li, P. Li, and T. Randak, "Evaluating the toxicity of environmental concentrations of waterborne chromium (VI) to a

model teleost, *Oncorhynchus mykiss*: a comparative study of in vivo and in vitro," *Comparative Biochemistry and Physiology C: Toxicology and Pharmacology*, vol. 153, no. 4, pp. 402–407, 2011.

[33] F. Di Natale, A. Erto, A. Lancia, and D. Musmarra, "Equilibrium and dynamic study on hexavalent chromium adsorption onto activated carbon," *Journal of Hazardous Materials*, vol. 281, pp. 47–55, 2015.

[34] B. D. Yirsaw, M. Megharaj, Z. Chen, and R. Naidu, "Reduction of hexavalent chromium by green synthesized nano zero valent iron and process optimization using response surface methodology," *Environmental Technology Innovation*, vol. 5, pp. 136–147, 2016.

[35] W. S. Hummers Jr. and R. E. Offeman, "Preparation of graphitic oxide," *Journal of the American Chemical Society*, vol. 80, no. 6, p. 1339, 1958.

[36] C. Hintze, K. Morita, R. Riedel, E. Ionescu, and G. Mera, "Facile sol-gel synthesis of reduced graphene oxide/silica nanocomposites," *Journal of the European Ceramic Society*, vol. 36, no. 12, pp. 2923–2930, 2016.

[37] A. Fasolino, J. H. Los, and M. I. Katsnelson, "Intrinsic ripples in graphene," *Nature Materials*, vol. 6, no. 11, pp. 858–861, 2007.

[38] S. Park, J. An, R. D. Piner et al., "Aqueous suspension and characterization of chemically modified graphene sheets," *Chemistry of Materials*, vol. 20, no. 21, pp. 6592–6594, 2008.

[39] T. Szabó, O. Berkesi, P. Forgó et al., "Evolution of surface functional groups in a series of progressively oxidized graphite oxides," *Chemistry of Materials*, vol. 18, no. 11, pp. 2740–2749, 2006.

[40] S. Haeri, B. Ramezanzadeh, and M. Asghari, "A novel fabrication of a high performance SiO_2-graphene oxide (GO) nanohybrids: characterization of thermal properties of epoxy nanocomposites filled with SiO_2-GO nanohybrids," *Journal of Colloid and Interface Science*, vol. 493, pp. 111–122, 2017.

[41] Y. Xu, H. Bai, G. Lu, C. Li, and G. Shi, "Flexible graphene films via the filtration of water-soluble noncovalent functionalized graphene sheets," *Journal of the American Chemical Society*, vol. 130, no. 18, pp. 5856-5857, 2008.

[42] W. Leng, M. Chen, S. Zhou, and L. Wu, "Capillary force induced formation of monodisperse polystyrene/silica organic-inorganic hybrid hollow spheres," *Langmuir*, vol. 26, no. 17, pp. 14271–14275, 2010.

[43] B. Ramezanzadeh, Z. Haeri, and M. Ramezanzadeh, "A facile route of making silica nanoparticles-covered graphene oxide nanohybrids (SiO_2-GO); fabrication of SiO_2-GO/epoxy composite coating with superior barrier and corrosion protection performance," *Chemical Engineering Journal*, vol. 303, pp. 511–528, 2016.

[44] L. Du, J. Tan, K. Wang, Y. Lu, and G. Luo, "Controllable preparation of SiO2 nanoparticles using a microfiltration membrane dispersion microreactor," *Industrial and Engineering Chemistry Research*, vol. 50, no. 14, pp. 8536–8541, 2011.

[45] T. H. T. Vu, T. T. T. Tran, H. N. T. Le et al., "Solvothermal synthesis of Pt -SiO_2/graphene nanocomposites as efficient electrocatalyst for methanol oxidation," *Electrochimica Acta*, vol. 161, pp. 335–342, 2015.

[46] P. Miretzky and A. F. Cirelli, "Cr(VI) and Cr(III) removal from aqueous solution by raw and modified lignocellulosic materials: a review," *Journal of Hazardous Materials*, vol. 180, no. 1–3, pp. 1–19, 2010.

[47] W. Jin, H. Du, S. Zheng, and Y. Zhang, "Electrochemical processes for the environmental remediation of toxic Cr(VI): a review," *Electrochimica Acta*, vol. 191, pp. 1044–1055, 2016.

[48] World Health Organization, *Guidelines for Drinking water Quality*, World Health Organization, Geneva, Switzerland, 2011.

[49] K. D. Kim and H. T. Kim, "Formation of silica nanoparticles by hydrolysis of TEOS using a mixed semi-batch/batch method," *Journal of Sol-Gel Science and Technology*, vol. 25, no. 3, pp. 183–189, 2002.

[50] Y. Zhou, Q. Bao, L. A. L. Tang, Y. Zhong, and K. P. Loh, "Hydrothermal dehydration for the "green" reduction of exfoliated graphene oxide to graphene and demonstration of tunable optical limiting properties," *Chemistry of Materials*, vol. 21, no. 13, pp. 2950–2956, 2009.

[51] D. Li, M. B. Müller, S. Gilje, R. B. Kaner, and G. G. Wallace, "Processable aqueous dispersions of graphene nanosheets," *Nature Nanotechnology*, vol. 3, no. 2, pp. 101–105, 2008.

[52] V. C. Tung, M. J. Allen, Y. Yang, and R. B. Kaner, "High-throughput solution processing of large-scale graphene," *Nature Nanotechnology*, vol. 4, no. 1, pp. 25–29, 2009.

[53] X. Fan, W. Peng, and Y. Li, "Deoxygenation of exfoliated graphite oxide under alkaline conditions: a green route to graphene preparation," *Advanced Materials*, vol. 20, no. 23, pp. 4490–4493, 2008.

[54] Y. Chang, S. Chen, and A. Cao, "Mechanism of Pressure-Accelerated Solvothermal Reduction of Graphene Oxide," *Journal of Shanghai University (Natural Science Edition)*, vol. 6, p. 8, 2010.

[55] M. Wang, J. Oh, T. Ghosh et al., "An interleaved porous laminate composed of reduced graphene oxide sheets and carbon black spacers by in situ electrophoretic deposition," *RSC Advances*, vol. 4, no. 7, pp. 3284–3292, 2014.

[56] T. Karthikeyan, S. Rajgopal, and L. R. Miranda, "Chromium(VI) adsorption from aqueous solution by *Hevea Brasilinesis* sawdust activated carbon," *Journal of Hazardous Materials*, vol. 124, no. 1–3, pp. 192–199, 2005.

[57] D. C. Sharma and C. F. Forster, "The treatment of chromium wastewaters using the sorptive potential of leaf mould," *Bioresource Technology*, vol. 49, no. 1, pp. 31–40, 1994.

[58] M. Kobya, "Removal of Cr(VI) from aqueous solutions by adsorption onto hazelnut shell activated carbon: kinetic and equilibrium studies," *Bioresource Technology*, vol. 91, no. 3, pp. 317–321, 2004.

[59] P. S. Rao and G. S. Manjunatha, "Kinetic Studies on Adsorption of Chromium by Coconut Shell Carbons from Synthetic Effluents," *Journal of Environmental Science and Health. Part A: Environmental Science and Engineering and Toxicology*, vol. 27, no. 8, pp. 2227–2241, 1992.

[60] K. Selvi, S. Pattabhi, and K. Kadirvelu, "Removal of Cr(VI) from aqueous solution by adsorption onto activated carbon," *Bioresource Technology*, vol. 80, no. 1, pp. 87–89, 2001.